Title
NEDD9 targets COL3A1 to promote endothelial fibrosis and pulmonary arterial hypertension

Journal
Science Translational Medicine, 10(445)

ISSN
1946-6234

Authors
Samokhin, Andriy O
Stephens, Thomas
Wertheim, Bradley M
et al.

Publication Date
2018-06-13

DOI
10.1126/scitranslmed.aap7294

Peer reviewed

HHS Public Access

Author manuscript

Sci Transl Med. Author manuscript; available in PMC 2018 December 13.

Published in final edited form as:

Sci Transl Med. 2018 June 13; 10(445): . doi:10.1126/scitranslmed.aap7294.

NEDD9 targets *COL3A1* to promote endothelial fibrosis and pulmonary arterial hypertension

Andriy O. Samokhin, Ph.D.[1], **Thomas Stephens, B.A.**[1], **Bradley M. Wertheim, M.D.**[1,2], **Rui-Sheng Wang, Ph.D.**[3], **Sara O. Vargas, M.D.**[4], **Lai-Ming Yung, Ph.D.**[5], **Minwei Cao, B.A.**[1], **Marcel Brown, B.A.**[1], **Elena Arons, M.D.**[1], **Paul B. Dieffenbach, M.D.**[2], **Jason G. Fewell, Ph.D.**[6], **Majed Matar, Ph.D.**[6], **Frederick P. Bowman, B.A., A.L.M.**[1], **Kathleen J. Haley, M.D.**[2], **George A. Alba, M.D.**[7], **Stefano M. Marino, Ph.D.**[8,9], **Rahul Kumar, Ph.D.**[10], **Ivan O. Rosas, M.D.**[2], **Aaron B. Waxman, M.D., Ph.D.**[2], **William M. Oldham, M.D., Ph.D.**[2], **Dinesh Khanna, M.D.**[11], **Brian B. Graham, M.D.**[10], **Sachiko Seo, M.D.**[12], **Vadim N. Gladyshev, Ph.D.**[8], **Paul B. Yu, M.D., Ph.D.**[5], **Laura E. Fredenburgh, M.D.**[2], **Joseph Loscalzo, M.D., Ph.D.**[1,5], **Jane A. Leopold, M.D.**[5], and **Bradley A. Maron, M.D.**[5,*]

[1]Department of Medicine, Brigham and Women's Hospital, Boston, MA, 02115 USA

[2]Division of Pulmonary and Critical Care Medicine, Brigham and Women's Hospital, Boston, MA, 02115 USA

[3]Channing Division of Network Medicine, Brigham and Women's Hospital, Boston, MA, 02115 USA

[4]Department of Pathology, Boston Children's Hospital, Boston, MA, 02115 USA

[5]Department of Medicine, Division of Cardiovascular Medicine, Brigham and Women's Hospital, Boston, MA, 02115 USA

[6]Celsion Corporation, Lawrenceville, NJ, 08648 USA

[7]Department of Pulmonary and Critical Care Medicine, Massachusetts General Hospital, Boston, MA, 02114 USA

[*]Corresponding author. bmaron@bwh.harvard.edu.

Author contributions:

Experiments involving cell biology or other in vitro analyses were performed by A.O.S., T.S., M.C., M.B., E.A., F.P.B., G.A.A., and B.A.M. Experiments involving computational analyses of NEDD9 cysteines were performed by S.M.M., V.G., B.A.M. Experiments involving microscale thermophoresis were performed or reviewed by A.O.S., W.M.O., J.L., and B.A.M. Experiments involving analysis of samples from animals or humans were performed, supervised or supported by A.O.S., B.M.W., S.O.V., L-M Y., E.A., K.J.H., R.K., I.O.R., A.B.W., P.B.Y., D.K., B.B.G., and B.A.M. Staramine reagent was purified and validated by J.G.F. and M.M. Transgenic NEDD9 embryos were supplied by S.S. Experiments involving systems biology and network analyses were performed by R-S W., B.A.M., and J.L. Experiments involving atomic force microscopy were performed or supervised by A.O.S., P.B.D., L.E.F., and B.A.M. The manuscript was drafted, reviewed, and revised by all authors, particularly A.O.S., J.A.L., J.L., and B.A.M.

Competing interests: There are no patents to disclose that are relevant to this work. B.A.M. initiated research supported by Gilead Sciences Inc. D.K.: investigator-initiated grants from BMS, Bayer, and Pfizer; acts as a consultant to Actelion, Boehringer Ingelheim, BMS, Bayer, Corbus, CSL Behring, Cytori, Eicos, GSK, Genentech/Roche, Sanofi, UCB.

Data and materials availability: Human pulmonary artery endothelial cells from patients with PAH are available from the PHBI under a material transfer agreement with the PHBI. Dermal fibroblasts from patients with systemic sclerosis are available from Dr. Dinesh Khanna under a material transfer agreement with the University of Michigan. The RNSASEQ data discussed in this publication have been deposited in NCBI's Gene Expression Omnibus and are accessible through GEO Series accession number GSE113659 (https://www.ncbi.nlm.nih.gov/geo/query/acc.cgi?acc=GSE113659). Inquiries for access or review of the primary data should be addressed to the corresponding author using the contact information provided within the manuscript.

[8]Department of Medicine, Division of Genetics, Brigham and Women's Hospital, Boston, MA, 02115 USA

[9]Department of Biotechnology, Akdeniz University, Konyaaltı, Antalya, 07058 Turkey

[10]Program in Translational Lung Research, Department of Medicine, Anschutz Medical Campus, Aurora, CO, 80045 USA.

[11]Division of Rheumatology, University of Michigan Scleroderma Program, Ann Arbor, MI, 48109 USA

[12]Department of Hematology & Oncology National Cancer Research Center East, Kashiwa-shi, Chiba-ken, 277-8577 Japan

Abstract

Germline mutations involving small mothers against decapentaplegic-transforming growth factor-β (SMAD-TGF-β) signaling are an important but rare cause of pulmonary arterial hypertension (PAH), which is a disease characterized, in part, by vascular fibrosis and hyperaldosteronism (ALDO). Here, we developed and analyzed a fibrosis protein-protein network (fibrosome) in silico, which predicted that the SMAD3 target neural precursor cell expressed developmentally down-regulated 9 (NEDD9) is a critical ALDO-regulated node underpinning pathogenic vascular fibrosis. Bioinformatics and microscale thermophoresis demonstrated that oxidation of Cys18 in the SMAD3 docking region of NEDD9 impairs SMAD3-NEDD9 protein-protein interactions in vitro. This effect was reproduced by ALDO-induced oxidant stress in cultured human pulmonary artery endothelial cells (HPAECs), resulting in impaired NEDD9 proteolytic degradation, increased NEDD9 complex formation with Nk2 homeobox 5 (NKX2–5), and increased NKX2–5 binding to *COL3A1*. Upregulation of NEDD9-dependent collagen III expression corresponded to changes in cell stiffness measured by atomic force microscopy. HPAEC-derived exosomal signaling targeted NEDD9 to increase collagen I/III expression in human pulmonary artery smooth muscle cells, identifying a second endothelial mechanism regulating vascular fibrosis. ALDO-NEDD9 signaling was not affected by treatment with a TGF-β ligand trap, and, thus, was not contingent on TGF-β-signaling. Colocalization of NEDD9 with collagen III in HPAECs was observed in fibrotic pulmonary arterioles from PAH patients. Furthermore, *NEDD9* ablation or inhibition prevented fibrotic vascular remodeling and pulmonary hypertension in animal models of PAH in vivo. These data identify a critical TGF-β-independent post-translational modification that impairs SMAD3-NEDD9 binding in HPAECs to modulate vascular fibrosis and promote PAH.

One Sentence Summary:

TGF-β-independent oxidative modification of NEDD9 at Cys18 promotes vascular fibrosis and the pathobiology of pulmonary arterial hypertension.

INTRODUCTION

Activation of small mothers against decapentaplegic (SMAD)-2/3 signal transduction through stimulation of the transforming growth factor-β receptor-II (TGF-β-RII) complex is a principal mechanism underlying transcriptional regulation of genes coding for collagen

(1). However, perturbations to TGF-β biofunctionality are associated with collagen deposition patterns that vary across cell types (2), and within patients who share circumspect clinical phenotypes (3). This heterogeneity suggests that the TGF-β 'master switch' theory may be an insufficient construct by which to understand fibrosis globally. Nonetheless, little is established on TGF-β-independent and cell-specific molecular mechanisms that control collagen synthesis to promote fibrosis in human disease.

Pulmonary arterial hypertension (PAH) is characterized, in part, by a fibrotic vasculopathy in pulmonary arterioles, which promotes early right heart failure and death (4). In PAH, endothelial dysfunction and vascular fibrosis are key pathogenic events that occur concurrently with changes in the normal cellular redox potential. Prior association studies imply a positive correlation between oxidant stress and collagen I/III protein synthesis via TGF-β in pulmonary endothelial cells in vitro (5), or upregulated endothelial mesenchymal transition (EndMT) in subpopulations of cells in remodeled PAH vessels in vivo (6). However, transgenic experimental PAH models or PAH patients harboring germline mutations that exaggerate TGF-β signaling express an angioproliferative-dominant phenotype with inconsistent vascular fibrosis patterns (7). Collectively, these data suggest there may be alternative or parallel redox-sensitive molecular mechanisms in endothelial cells that contribute to fibrosis in PAH.

In PAH patients, overactivation of the renin-angiotensin axis is associated with elevated concentrations of the mineralocorticoid hormone aldosterone (ALDO) (8), which correlate positively with hemodynamic measures of vascular remodeling (9). Pathophysiological aldosterone concentrations observed in PAH are sufficient to perturb the normal redox potential of cultured pulmonary artery endothelial cells by direct activation of the reactive oxygen species generating enzyme NOX4 (10). However, stimulation of the mineralocorticoid receptor by ALDO is implicated in both adaptive wound healing in skin and pathogenic vascular fibrosis in PAH (5, 11). This observation suggests that there is substantial overlap among ALDO signaling pathways irrespective of fibrosis subtype. To address this knowledge gap, we hypothesized that applying Bayesian (conditional probability) analytical methods to ALDO gene targets segregated by distinct fibrosis functionalities would enable the discovery of unknown PAH-specific fibrogenic mechanisms, which may be independent of TGF-β signaling.

RESULTS

NEDD9 is a critical network node distinguishing fibrosis subtypes

Network medicine is an analytical approach to studying the relationships among molecular interactions that may be important in diseases, and was used in this study to identify critical genes regulated by ALDO that account for protein-protein connectivity involving adaptive and pathogenic fibrosis phenotypes. Fibrosis seed genes that are focused on interactions associated with dermal (adaptive) fibrosis and vascular (pathogenic) fibrosis were selected from GeneCards. Because of our focus on PAH as a human disease correlate to these in silico analyses, we excluded genes that were associated with lung fibrosis in particular (n = 362) to avoid studying pathways relevant to idiopathic pulmonary fibrosis or other fibrotic parenchymal lung diseases (Fig. 1A). The gene products (proteins) of the remaining fibrosis

genes were mapped to the consolidated human protein-protein interactome (CHI) (12) to generate a network of fibrosis protein-protein interactions. The resulting fibrosome had 315 proteins nodes and 1,171 interactions (Fig. 1B and expanded view in fig. S1A).

We also incorporated a total of 130 ALDO-regulated genes in human vascular endothelial cells expressing the mineralocorticoid receptor (13). Thus, the proteins corresponding to 246 adaptive fibrosis genes, 236 pathogenic fibrosis genes, and 86 ALDO-regulated genes in total were mapped to the CHI. Compiling the fibrosis and ALDO-regulated gene products generated a subnetwork, the ALDO-fibrosome, that included 348 protein nodes and 1,236 interactions (fig. S1B). To emphasize the connectivity involving ALDO-regulated genes, the ALDO-fibrosome network was modified to exclude the connections between fibrosis nodes exclusively (Fig. 1C and expanded view in fig. S1C).

Next, betweenness centrality (BC) was used to focus on pathways regulated by ALDO that are likely to perform a critical function in the fibrosis phenotype transition, and, thus, permit identification of critical nodes distinguishing adaptive from pathogenic fibrosis in silico. Using this approach, neural precursor cell expressed developmentally down-regulated 9 (NEDD9) emerged from our analysis. Specifically, NEDD9 was assigned a top BC score ($P = 0.004$ versus other ALDO-regulated genes; $P = 7.5 \times 10^{-7}$ versus random network) (Fig. 1D). Of the proteins with high BC scores, NEDD9 was selected for further analysis based on its previously reported role in clinical phenotypes that overlap with PAH, such as connective tissue disease (14), converging lines of evidence in tumorigenic cells lines that have indirectly implicated negative regulation of NEDD9 by SMAD3 via proteolytic degradation (15), and lack of data on the role of NEDD9 in primary cardiopulmonary diseases.

NEDD9-Cys18 regulates NEDD9-SMAD3 binding in vitro

Oxidative modification of Src Homology (SH) domain cysteinyl thiols has been shown to regulate linkage between Crk-associated substrate (Cas) proteins and binding partners (16). We used computational analyses to predict that among 10 protein cysteinyl thiols, Cys18 in the NEDD9 SH3 domain is the most prone to react with an oxidant based on the pKa (6.65) and accessible surface area (17.5 $Å^2$) of its sulfur atom (fig. S2A). Using microscale thermophoresis, co-incubation of purified human wild type (WT) NEDD9 and SMAD3 with hydrogen peroxide (H_2O_2) (500 μM) diminished WT-NEDD9-SMAD3 binding, whereas a mutant NEDD9 containing an alanine-for-cysteine substitution at position 18 (NEDD9-C18A) did not show impaired protein-protein interactions with SMAD3 (Fig. 2A,B). Directionally similar effects were observed by oxidant stress on NEDD9-SMAD3 binding in COS-7 cells transfected with cDNA coding SMAD3 and WT-NEDD9 or NEDD9-C18A (Fig. 2C and fig. S2B,C).

We confirmed that H_2O_2 treatment oxidatively modified NEDD9-Cys18 to sulfonic acid (SO_3H) by in-tandem liquid chromatography-mass spectrometry (LC-MS) (Fig. 2D). Lysates from human pulmonary artery endothelial cells (HPAECs) treated with ALDO, which stimulates NOX4 to increase reactive oxygen species accumulation (10), or H_2O_2, demonstrated increased NEDD9-SOH by 56% ($P < 0.02$) and 106% ($P = 0.026$), respectively. Furthermore, NEDD9-SOH induced by ALDO or H_2O_2 was associated with a

decrease in SMAD3 binding to NEDD9 by 66% ($P = 0.04$) and 54% ($P < 0.02$), respectively (Fig. 2E).

Decreased NEDD9-SMAD3 binding promotes NEDD9-dependent fibrosis

Treatment with ALDO or hypoxia (FiO_2 2%), which has been shown previously to induce ALDO synthesis in HPAECs (5), increased NEDD9 expression (Fig. 3A). We also observed no significant effect by ALDO on NEDD9 mRNA expression in HPAECs ($P = 0.43$, fig. S3A), providing further evidence in favor of posttranscriptional regulation of NEDD9 by oxidant stress. Treatment with spironolactone decreased NEDD9 in ALDO- and hypoxia-treated HPAECs by 44% ($P < 0.04$) and 42% ($P = 0.03$), respectively, indicating that upregulation of NEDD9 by ALDO involves mineralocorticoid receptor signaling. Although TGF-β-RII is a downstream target of ALDO reported previously to regulate NEDD9 in epithelial cancer cell lines (15), pre-treatment with a TGF-β−1/3 ligand trap to inhibit bioactive TGF-β did not affect NEDD9 expression significantly in ALDO-treated HPAECs ($P = 0.60$) (Fig. 3B). However, a time-dependent effect on NEDD9 accumulation was observed by the proteasome inhibitor MG-132 or by H_2O_2 (fig. S3B,C), and combining these treatments increased NEDD9 expression maximally (Fig. 3C). By contrast, ALDO or hypoxia did not affect NEDD9 in dermal microvascular endothelial cells, dermal fibroblasts, or keloid fibroblasts, which are cell types associated with adaptive fibrosis and excessive, benign fibroblast proliferation, respectively, or in other cell types associated with arterial remodeling (fig. S4A–F).

We next aimed to validate our network findings suggesting that NEDD9 regulation by ALDO is important in vascular fibrosis. RNASEQ next generation sequencing was performed on RNA isolated from ALDO-treated HPAECs that were transfected with siRNA to NEDD9 (si-NEDD9) or untransfected (fig. S5A,B and data file S1). Compared to untransfected cells, si-NEDD9 decreased expression of various genes implicated in collagen synthesis, matrix remodeling, or PAH, including *COL1A1,2* and *BMPR1A* (table S1). RNASEQ also showed that mRNA transcript quantity of collagen III, which is the principal fibril-forming collagen in cardiovascular disease, was increased significantly in HPAECs treated with ALDO compared to vehicle control (Fold change [FC] = +2.47, $n = 3–6$ samples from female and male donors, multiple-test corrected P value, False discovery rate [FDR] = 0.016, $P = 0.001$) (data file S2). However, this effect was inhibited by transfection with si-NEDD9 (FC = +1.78 in si-NEDD9+ALDO versus vehicle, $n = 3–6$ samples from female and male donors, multiple-test corrected P value, FDR = 0.250, $P = 0.07$) (data file S3).

The transcription factor Nk2 homeobox 5 (NKX2–5) is predicted to target *COL3A1*, and we observed NEDD9 expression in the nucleus of HPAECs with or without ALDO treatment, and in the nucleus of HPAECs isolated from PAH patients (PAH-HPAECs) (fig. S5C,D and Movie S1–3). ALDO increased nuclear colocalization (fig. S6A) and co-immunoprecipitation of NKX2–5 with NEDD9 (Fig. 3D). We also observed an inverse relationship between amount of the NEDD9-SMAD3 complex and NEDD9-NKX2–5 complex ($r = −0.91$, $P < 0.01$), as well as a positive correlation between amount of NEDD9 and the NEDD9-NKX2–5 complex ($r = +0.86$, $P = 0.03$) (fig. S6B). These findings were

consistent with our observation that si-NEDD9 decreased NKX2–5 without significantly influencing SMAD3 expression ($P = 0.75$) (fig. S6C), and, overall, show that impaired SMAD3 association with NEDD9 promotes NEDD9 stability, which, in turn, permits greater NEDD9-NKX2–5 interaction. Transfection with si-SMAD3 (fig. S6D) increased NEDD9-NKX2–5 co-immunoprecipitation under basal conditions and in ALDO-treated HPAECs (Fig. 3E). ALDO increased NKX2–5 binding to the *COL3A1* gene as well as COL3A1 mRNA transcript quantity, which was inhibited significantly by si-NEDD9 ($P = 0.046$) and si-NKX2–5 ($P < 0.001$), respectively (Fig. 3F and fig. S6E,F).

We next analyzed the functional consequences of increased NEDD9 on *COL3A1* gene transcription in ALDO-treated HPAECs. Molecular inhibition of NEDD9 attenuated the ALDO-induced increased collagen III expression, matrix metalloproteinase-2 proteolytic activity, 3-dimensional collagen matrigel contraction, and cell stiffness (Fig. 3G–J). In contrast, overexpression of NEDD9 correlated positively with collagen III expression in HPAECs (fig. S7A). Pro-fibrotic changes to HPAECs by ALDO (fig. S7B) included a distinctive “net” pattern of collagen stranding in HPAECs that was not evident in human pulmonary artery smooth muscle cells (HPASMCs) or normal human lung fibroblasts (NHLFs) (fig. S7C). In addition, an ALDO-induced fibrotic phenotype in HPAECs was observed without differences in expression of von Willebrand factor (vWF), vascular endothelial cadherin (VE-cadherin), platelet endothelial cell adhesion molecule-1 (PECAM-1), or the EndMT markers twist-related protein 1 (TWIST) and α-smooth muscle actin (SMA) (fig. S7C,D).

NEDD9 is increased and co-localizes with collagen III in PAH-HPAECs

To determine the relevance of our in silico and in vitro findings to PAH in vivo, we analyzed NEDD9 and collagen III expression in remodeled pulmonary arterioles from PAH patients and animal models characterized by ALDO, overactivation of TGF-β signaling, or vascular reactive oxygen species accumulation (10, 17, 18). We observed an increase in NEDD9, collagen III, and NEDD9-collagen III co-localization in lung tissue from IL-6(TG+) PAH and *Schistosoma mansoni*-PAH mice; SU-5416/Hypoxia-PAH and monocrotaline (MCT)-PAH rats; and from patients with PAH (Fig. 4A and fig. S8).

Compared to control, we also observed a significant increase in NEDD9-positivity in PAH-HPAECs ($P < 0.001$) (Fig. 4B), which included NEDD9 expression in the nucleus of cells (fig. S5D and Movie S3), and correlated positively with collagen III quantity measured by volumetric analysis ($r = +0.78$, $P = 0.02$) (fig. S8C). Compared to control, PAH-HPAECs expressed significantly higher concentrations of the NEDD9-NKX2–5 complex ($P < 0.02$) and lower concentrations of the NEDD9-SMAD3 complex ($P = 0.04$) (Fig. 4B), providing a translational correlate to our data implicating endothelial NKX2–5-COL3A1 signaling. This conclusion was supported further by findings in situ demonstrating increased collagen III co-localization with vWF-positive cells in remodeled arterioles from PAH patients compared to controls (Fig. 4C). Furthermore, oxidative modification of NEDD9-Cys18 to cysteinyl sulfonic acid was confirmed by LC-MS in PAH-HPAECs in the absence of exogenous oxidant stress (fig. S9). Although our observations in vitro demonstrated that upregulation of NEDD9-collagen III was specific to HPAECs, immunohistochemical studies showed

increased NEDD9 expression globally in remodeled pulmonary arterioles from PAH patients, which was not evident in specimens from idiopathic pulmonary fibrosis and malignancy patients or healthy control (fig. S10).

HPAEC-derived exosomes regulate NEDD9 in pro-fibrotic vascular cells

Our findings in PAH patients suggest diffuse upregulation of NEDD9 in fibrotic pulmonary arterioles; however, ALDO did not increase NEDD9 expression in HPASMCs or other fibrogenic vascular cell types in vitro. Therefore, we explored the possibility that treating HPAECs with ALDO induces NEDD9 expression in HPASMCs through a mechanism involving paracrine signaling. In a co-culture system where HPAECs were grown on the upper position of the co-culture apparatus insert plate, NEDD9 expression was analyzed in HPASMCs. ALDO increased NEDD9 expression by 1.9-fold ($P = 0.02$) and 2.0-fold ($P = 0.01$) when HPASMCs were co-cultured with HPAECs (Fig. 5A).

We next explored exosome-mediated crosstalk between cells as a mechanism by which to account for this effect, and observed co-localization of the exosome marker CD9 with NEDD9 (fig. S11A) and NEDD9 with DAPI staining in HPASMCs and NHLFs treated with exosomes from ALDO-treated HPAECs (exo-ALDO-HPAEC) (fig. S11B). Compared to untreated cells or exosomes from vehicle-treated HPAECs, NEDD9 positivity was increased significantly in HPASMCs, NHLFs, or dermal fibroblasts from systemic sclerosis patients treated with exo-ALDO-HPAEC ($P \leq 0.03$ for all comparisons) (Fig. 5B,C). In HPASMCs, exo-ALDO-HPAEC increased collagen I expression significantly ($P < 0.02$) (Fig. 5D). However, this effect was not mediated by TGF-β; compared to exosomes from HPAECs treated with vehicle, no significant changes in TGF-β large latent complex (TGF-β-LLC) expression were observed in exo-ALDO-HPAECs ($P = 0.16$) (Fig. 5E), nor was there evidence of endothelial NEDD9 release into the culture medium of vehicle- or ALDO-treated cells by LC-MS (fig. S12).

Inhibition of NEDD9 prevents PAH in vivo

We next tested whether NEDD9 is a target by which to modulate pulmonary arterial fibrosis and improve pulmonary hypertension in PAH in vivo. NEDD9-deficient transgenic mice (fig. S13A) were studied using the SU-5416/Hypoxia model of PAH, which among murine models is characterized by severe vascular fibrosis. Compared to WT-SU-5416/Hypoxia, we found that NEDD9$^{+/-}$-SU-5416/Hypoxia and NEDD9$^{-/-}$-SU-5416/Hypoxia mice had decreased right ventricular systolic pressure (RVSP) by cardiac catheterization (38.4 ± 2.9 versus 31.1 ± 0.9 versus 28.9 ± 1.1 mmHg, $P < 0.001$) and RV mass by Fulton index (0.37 ± 0.01 versus 0.31 ± 0.02 versus 0.28 ± 0.02 g, $P < 0.001$), which corresponded to a decrease in endothelial collagen III expression and pulmonary arterial collagen burden (Fig. 6A,B). Overall, we observed strong correlation between pulmonary arterial collagen level and RVSP (r= +0.98, $P < 10^{-5}$) (fig. S13B), implicating NEDD9-dependent fibrosis as a key determinant of pulmonary hypertension in this model of PAH.

We next studied MCT-PAH rats owing to prior reports showing ALDO, increased oxidant stress, substantial pulmonary vascular fibrosis in this model (5). Proximity ligation assay demonstrated elimination of the physical association of NEDD9 with SMAD3 in remodeled

pulmonary arterioles of MCT-PAH rats compared to controls (fig. S13C). Staramine-mPEG (19) labeled with si-NEDD9 decreased NEDD9 and collagen III expression in PAECs from MCT-PAH rats (Fig. 6C). This treatment prevented hypertrophic remodeling and fibrillar collagen deposition in distal pulmonary arterioles assessed by anti-α-SMA immunohistochemistry, Picrosirius Red staining, and Gomori Trichrome staining (Fig. 6D and fig. S13D,E).

The favorable effects of NEDD9 inhibition on vascular remodeling in MCT-PAH normalized RVSP (80 ± 9 versus 28 ± 3 mmHg, $P < 0.001$), indexed pulmonary vascular resistance (7.3 ± 2.3 versus 1.8 ± 0.3 Wood units, $P = 0.02$) (Fig. 6E), and RV-pulmonary arterial coupling (1.6 ± 0.2 versus 0.6 ± 0.02 Ees/Ea, $P < 0.01$) (Fig. 6F). Taken together, these data demonstrate that NEDD9 is a modifiable treatment target by which to improve fibrotic pulmonary vascular remodeling and cardiopulmonary hemodynamics as shown in two animal models of PAH.

DISCUSSION

From our network analysis emphasizing tissue-specific pathways involved in fibrogenesis, the Cas protein NEDD9 emerged as a critical node regulating collagen pathogenicity. Redox regulation of NEDD9 at Cys18 impaired the physical interaction between SMAD3 and NEDD9, which in HPAECs stabilized NEDD9 by inhibiting its proteolytic degradation. Increased bioavailable NEDD9 was not contingent on TGF-β but induced NKX-2–5 binding to the *COL3A1* gene, resulting in pulmonary endothelial fibrosis. Endothelial exosomes target other pro-fibrotic pulmonary vascular cells to increase NEDD9 and fibrillar collagen, which is consistent with our finding that NEDD9 expression is increased globally in remodeled pulmonary arterioles from PAH patients. Genetic ablation or molecular inhibition of *NEDD9* decreased pulmonary vascular fibrosis and improved vascular resistance in experimental PAH in vivo. Overall, these data demonstrate TGF-β-independent regulation of collagen synthesis through posttranscriptional oxidative modification of NEDD9-Cys18, and illustrate two endothelium-dependent molecular mechanisms underpinning pulmonary vascular fibrosis in PAH.

Comparative analyses between fibrosis subtypes using unbiased methods are lacking, despite substantial overlap among signaling pathways reported to regulate collagen of varying functionality, tissue involvement, and clinical phenotypes. In this study, we developed an innovative network strategy in which a unique fibrosome derived from the CHI was analyzed, using betweenness centrality to identify important pathways regulating the transition between functionally distinct forms of fibrosis. We found that a series of nodes (of which we focused on NEDD9) were transitional between these fibrosis subtypes, which provides key insight on the alignment between molecular pathways regulating collagen deposition and collagen function. This result supports a paradigm shift in which disease-specific mechanisms are emphasized in addition to collagen quantification as key metrics that are important but underutilized when characterizing fibrosis pathogenicity (20).

There are converging data implicating NEDD9 in the biology of solid tumors (21–22) and proliferative rheumatoid diseases (23), which in malignancy occurs primarily through focal

adhesion kinase (FAK)-mediated cell-cell adhesion, growth, and metastasis (24). Our findings expand on these observations by providing a comprehensive analysis of NEDD9 in cardiopulmonary disease, and identify NEDD9 as a heretofore-unrecognized mediator of vascular fibrosis with direct relevance to pulmonary hypertension. Of note, however, our data diverge from earlier reports in breast cancer cells which suggested bidirectional positive and negative feedback between TGF-β-R1 and NEDD9 (25). Here we show that oxidation of NEDD9-Cys18 by ALDO or oxidant stress decreased NEDD9-SMAD3 binding, which corresponded to impaired NEDD9 proteolysis and increased NEDD9 accumulation. Thus, NEDD9 protein stability, due to its dissociation from SMAD3, regulated the physical association of NKX2–5 to the *COL3A1* gene. NEDD9 inhibition prevented NKX2–5 binding to the *COL3A1* gene and Nxk2–5 inhibition decreased collagen III mRNA transcript quantity. This is consistent with data showing NEDD9 expression in the nucleus: in MCF-7 cultures, the endogenous NEDD9 fragment p55 localizes to mitotic spindle (26), and in the current study NEDD9 localization to the nucleus was observed in vehicle- and ALDO-treated HPAECs as well as PAH-HPAECs.

These data provide an alternative mechanism which accounts for the variability in fibrosis observed across PAH subgroups defined commonly by overactivation of TGF-β, including hereditable PAH from BMPR-2 mutation or *Schistosoma mansoni*-PAH, which was a model that was included in the current study. Our findings demonstrate that endothelial exosomes transduce the remodeling effect of ALDO on different vascular cell types. This, in turn, has important implications on understanding diffuse patterns of fibrosis in cardiac tissues and other targets of end-organ damage mediated by ALDO in many cardiopulmonary diseases, including the pulmonary circulation in PAH (5, 27).

Prior reports have identified vascular smooth muscle cells, adventitial fibroblasts, and endothelial cells via EndMT in the pathogenesis of vascular fibrosis in PAH (28, 29). Based on published work indicating that collagen synthesis in stimulated HPAECs occurs at a time point prior to EndMT onset (5), we focused on alternative (or parallel) mechanisms by which endothelial cells may contribute to fibrosis in the absence of phenotype switching. In this study, upregulation of NEDD9 by oxidant stress controlled HPAEC collagen net formation to increase cell stiffness without altering expression of EndMT proteins. This finding suggests that endothelial cells are independent contributors to collagen synthesis resulting in increased cell stiffness through NEDD9, and, thus identifies endothelial fibrosis as a critical PAH pathophenotype. Furthermore, endothelial exosomes from ALDO-treated HPAECs increased NEDD9 and collagen in other cell types associated with vascular fibrosis, including HPASMCs. This mechanism may also have direct relevance to other pro-fibrotic cell types, particularly adventitial fibroblasts, which are sensitive to paracrine signaling and regulate collagen deposition in PAH (30). Further investigations focusing on endothelial NEDD9 in early-stage disease, which is characterized by increased oxidant stress, endothelial injury, and vascular fibrosis (31), or as a target of circulating exosomes are warranted (32).

Epigenetic and post-transcriptional regulation of signaling pathways that control vascular structure and function are central to PAH (33). In HPAECs, ALDO increases reactive oxygen species accumulation, including H_2O_2, which is generated via the reduction of

superoxide anion spontaneously or via superoxide dismutases, or directly through a two-electron reduction of molecular oxygen catalyzed by NOX4. The sulfur atom of cysteinyl thiols may react with partially reduced oxygen species to form higher oxidative intermediaries that modify the conformational structure of proteins, impair G-protein coupled receptor signaling, or inhibit *S*-nitrosylation to modulate cardiovascular disease (34). However, prior reports in PAH have studied thiols with known biofunctionality, and tested the consequences of thiol oxidation indirectly (10). By contrast, computational modeling was used in this study to rank thiol reactivity based on pKa and access to oxidative insults, as predicted when analyzing proteins with NEDD9 structural homology. From this approach, Cys18 was identified as a redox-sensitive regulatory protein cysteinyl thiol, which was not based on *a priori* understanding of thiol biochemistry in NEDD9. Microscale thermophoresis provided definitive evidence on NEDD9-SMAD3 binding affinity and the contribution of Cys18 to the dynamics of this protein-protein interaction. Our observations in HPAECs show a time course-dependent increase in NEDD9 accumulation induced by H_2O_2 and that oxidation of NEDD9-Cys18 included the formation of cysteine sulfenic acid, which is a reversible modification. However, further experimentation is needed to determine if the redox switch at NEDD9-Cys18 is reversible, and if this bears on the therapeutic relevance of attenuating vascular oxidant stress in PAH.

Characterizing the redox regulation of NEDD9-SMAD3 may be relevant to a range of functionally essential pathways in PAH, including bone morphogenetic protein receptor-2 (BMPR-2) signaling. Indeed, our findings have implications for hereditary PAH, since vascular cells expressing a germline mutation in the *BMPR2* gene are predisposed to both increased oxidant stress (35) and increased SMAD3 (36). Under these circumstances, two parallel but independent pro-fibrotic signaling pathways relevant to PAH emerge through: i) oxidized NEDD9 and ii) increased bioactive SMAD3 that may occur due to the direct effects of *BMPR2* mutation or impaired NEDD9-SMAD3 binding.

Apoptosis resistance, dysregulated cell growth, and unopposed vascular proliferation contribute to the vasculopathy of PAH (37). Although NEDD9 has been linked to these processes in other cell types, and its inhibition improved hypertrophic remodeling in experimental PAH, the direct effect of NEDD9 on mitosis or cell survival was not investigated specifically in our study. Our data quantifying the EC_{50} for NEDD9-SMAD3 binding were limited by the maximum concentration of protein tested, and it is also possible that other NEDD9 thiols not analyzed in this study could exert functional effects on endothelial phenotype. Along these lines, alternative NEDD9-Cys18 post-translational modifications relevant to ALDO and PAH-HPAEC biology, including via cysteine reactivity with peroxynitrite and other reactive nitrogen species or formation of *S*-nitrosothiols, could affect NEDD9 stability and its bioactivity and merit further investigation.

We focused on NEDD9-dependent signaling involving SMAD3; however, crosstalk between SMAD3 and other SMAD isoforms, as well as TGF-β-connective tissue growth factor (CTGF) signaling, have been implicated in the pathobiology of pulmonary vascular fibrosis and PAH (37). Thus, additional studies in HPAECs are required to understand the effect of SMAD-SMAD interactions on proteolytic regulation of NEDD9, the effect of impaired NEDD9-SMAD3 binding on SMAD bioactivity, and NEDD9-independent pathways

regulating collagen. Further investigation is also needed to clarify the precise mechanism by which to account for redox regulation of NEDD9 selectively in HPAECs. This finding may be consistent with variability across cell types reported for intracellular reductive potential (38), subcellular compartmentalization of proteins (NEDD9) that affect exposure to oxidants (39, 40), and signaling responses to ALDO (5).

Although our seed genes were selected from the curated database, it was not possible to confirm that adaptive fibrosis genes were not also implicated in maladaptive processes, such as hypertrophic scar. In turn, including such pathways could have affected the validity and topology of our networks. Additionally, plasma or vascular ALDO concentrations were not available from the PAH patients, which could affect the translational relevance of our findings implicating ALDO-NEDD9-fibrosis signaling in vivo; however, the adverse effects of oxidant stress in PAH are well established and was a central mechanistic focus of this study. Experiments analyzing the effect of si-NEDD9 on PAH used a disease prevention experimental design, and, therefore, the therapeutic implications of our in vivo data require further investigation.

In summary, we identify NEDD9 as a contributor to pulmonary arterial fibrosis, vascular remodeling, and pulmonary hypertension in PAH. Our observations illustrate two previously unrecognized mechanisms underpinning endothelial regulation of vascular fibrosis: oxidative modification of NEDD9-Cys18 to increase *COL3A1* gene transcription in HPAECs and paracrine signaling mediated by HPAEC-exosomes to increase fibrillar collagen expression in pro-fibrotic target cells. Our findings on NEDD9-SMAD3 binding affinity also suggest that opportunity may exist to maintain normal NEDD9 proteolysis by inhibiting Cys18 oxidation and prevent fibrotic vascular remodeling. Collectively, these data suggest that NEDD9 mediates fibrotic vascular remodeling with potential therapeutic relevance for PAH patients.

MATERIALS AND METHODS

Study design

We hypothesized that systems biology could be used to identify disease-specific mechanisms underpinning pathogenic fibrosis, including vascular fibrotic remodeling in PAH. All data included in the manuscript were reproduced across multiple iterations of the same experiment, which were often performed on different days, replicated by different investigators involved in the project, and confirmed using multiple approaches. Cell culture experiments were performed at least 3 times, and at least in triplicate for each replicate when possible. For studies involving rats and mice, animals were randomly assigned to a treatment intervention. Power calculations for these studies were performed based on prior work (10, 17, 19). The number of animals needed in each treatment group was calculated to detect a 40% difference in pulmonary pressures with a 5% α-error and 80% power was used for performing experiments. For experiments involving human lung tissue, the number of samples included in each experiment was based largely on availability. Once conditions for an experiment were optimized, all data were included in the absence of a specific technical or procedural reason that confounded interpretation of a finding or if data met the pre-specified, standard outlier definition of |±| 2-S.D. of the mean. When possible for

experiments involving biochemistry, cell biology, and other in vitro assays, the senior author (B.A.M.) and other senior investigators (J.A.L.) involved in the project were blinded to the treatment conditions for initial data review/interpretation. A similar policy was used for blinding with respect to animal experiments; however, owing to the severity of vascular remodeling and pulmonary hypertension in experimental PAH and patients with PAH this was not possible uniformly.

Human lung samples

The experimental protocol included only discarded lung samples and was approved by the institutional review board at Brigham and Women's Hospital (IRB# 2015P001526; 2011P002419; 2001P000876) and Boston Children's Hospital (IRB# P00010717). Hematoxylin and eosin, elastin, and Gomori trichrome staining as well immunofluorescence (described in detail in the Supplementary Materials and Methods) were performed on distal pulmonary arterioles from formalin-fixed, paraffin-embedded archival lung specimens acquired by clinical experts in the field that confirmed accurate patient diagnosis as follows: lung explant for PAH (S.O.V.) or idiopathic pulmonary fibrosis (IPF) (I.O.R.); and, open lung biopsy to diagnose malignancy (S.O.V.) (table S2). Samples from controls without lung or pulmonary vascular disease were fully deidentified discarded donor lung samples provided by the New England Organ Bank (K.J.H.) (table S2).

Animal models of PAH

All animals were handled in accordance with US National Institutes of Health guidelines, and all procedures were approved by the local committees at Brigham and Women's Hospital and the University of Colorado. All animals were fed standard chow. Animal treatments and analyses were controlled and blinded, whenever possible. Additional details can be found in the Supplementary Materials and Methods.

Statistical analysis.

All analyses were performed using Origin 9.01, Graphpad Prism v7.03, and Cytoscape 3.5.1. Data are expressed as mean ± S.E.M. Comparison between two groups was performed by the Student's unpaired two-tailed t-test. For the analyses involving the proximity ligation assay and assessment of NEDD9 versus p130Cas expression using anti-NEDD9 Ab2: a signal was not detectable in the control group, and, therefore, a one-sample t-test was used to determine if results for the comparator group were statistically significant. One-way analysis of variance (ANOVA) was used to examine differences in response to treatments between groups. An analysis of covariance (ANCOVA) was used to examine differences between groups and control for the effect of continuous variables. *Post-hoc* analysis was performed by the method of Tukey. $P < 0.05$ was considered significant. For experiments with $n < 20$, individual data points are presented in the figure or are included in data file S4.

Supplementary Material

Refer to Web version on PubMed Central for supplementary material.

Acknowledgements:

The authors would like to acknowledge the Pulmonary Hypertension Breakthrough Initiative (PHBI) for access to cells, which is supported by an NHLBI #R24HL123767 and the Cardiovascular Medical Research and Education Fund (CMREF). We also wish to acknowledge Ronglih Liao, Ph.D. at Brigham and Women's Hospital for assistance in acquiring confocal microscope images, Ross Tomaino, Ph.D. at Harvard Medical School for assistance with LC-MS, Eliza Tsou, M.D. at the University of Michigan for assistance with harvesting DFBs from systemic sclerosis patients, Kelly Arnett, Ph.D. at the Center for Macromolecular Interactions at Harvard Medical School for assistance with the MST experiments, Manoj Bhasin, Ph.D. for assistance with RNASEQ experiments, and Christina Haeger, M.D. for assistance with the AFM experiments. This work was performed in part at the Center for Nanoscale Systems (CNS), a member of the National Nanotechnology Coordinated Infrastructure Network (NNCI), which is supported by the National Science Foundation under NSF award no. 1541959. CNS is part of Harvard University. The following reagent was provided by the NIAID Schistosomiasis Resource Center for distribution through BEI Resources, NIH-NIAID Contract HHSN272201000005I. NIH: Schistosoma mansoni, Strain NMRI, Exposed Swiss Webster Mice, NR-21963.

Funding: Relevant funding sources are as follows: B.A.M.: (NIH) 1K08HL11207-01A1 and R56HL131787, 1R01HL139613-01, American Heart Association (AHA 15GRNT25080016), Pulmonary Hypertension Association, CMREF, and Klarman Foundation at Brigham and Women's Hospital, Systemic Sclerosis Foundation; W.M.O.: (NIH) K08HL128802; G.A.A.: (NIH) 1F32HL139019-01; B.M.W.: (NIH) 5T32HL007633-32; J.A.L: (NIH/NHLBI) 1U01HL125215-01; J.L.: R37 HL061795, HL108630 (MAPGEN), U54 HL119145, PPG HL048743; D.F.B.: (NHLBI) F32HL131228; D.K.: (NIH/MIAMS) K24 AR063120, R01 ARO70470; P.B.Y.: (NIH) 5R01-HL131910; V.N.G.: (NIH) GM065204; L.E.F.: (NIH) R01HL114839.

REFERENCES

1. Daniels CE, Wilkes MC, Edens M, Kottom TJ, Murphy SJ, Limper AH, Leof EB, Imatinib mesylate inhibits the profibrogenic activity of TGF-beta and prevents bleomycin-mediated lung fibrosis. J Clin Invest 114, 1308–1316 (2004). [PubMed: 15520863]
2. Grafe I, Yang T, Alexander S, Homan EP, Lietman C, Jiang MM, Bertin T, Munivez E, Chen Y, Dawson B, Ishikawa Y, Weis MA, Sampath TK, Ambrose C, Eyre D, Bachinger HP, Lee B, Excessive transforming growth factor-beta signaling is a common mechanism in osteogenesis imperfecta. Nat Med 20, 670–675 (2014). [PubMed: 24793237]
3. Wei H, Hu JH, Angelov SN, Fox K, Yan J, Enstrom R, Smith A, Dichek DA, Aortopathy in a mouse model of Marfan Syndrome is not mediated by altered transforming growth factor-β signaling. J Am Heart Assoc 6,pii:e004968 (2017).
4. Maron BA, Galie N, Diagnosis, Treatment, and Clinical Management of Pulmonary Arterial Hypertension in the Contemporary Era: A Review. JAMA Cardiol 1, 1056–1065 (2016). [PubMed: 27851839]
5. Maron BA, Oldham WM, Chan SY, Vargas SO, Arons E, Zhang YY, Loscalzo J, Leopold JA, Upregulation of steroidogenic acute regulatory protein by hypoxia stimulates aldosterone synthesis in pulmonary artery endothelial cells to promote pulmonary vascular fibrosis. Circulation 130, 168–179 (2014). [PubMed: 25001622]
6. Ranchoux B, Antigny F, Rucker-Martin C, Hautefort A, Pechoux C, Bogaard HJ, Dorfmuller P, Remy S, Lecerf F, Plante S, Chat S, Fadel E, Houssaini A, Anegon I, Adnot S, Simonneau G, Humbert M, Cohen-Kaminsky S, Perros F, Endothelial-to-mesenchymal transition in pulmonary hypertension. Circulation 131, 1006–1018 (2015). [PubMed: 25593290]
7. Drake KM, Dunmore BJ, McNelly LN, Morrell NW, Aldred MA, Correction of nonsense BMPR2 and SMAD9 mutations by ataluren in pulmonary arterial hypertension. Am J Respir Cell Mol Biol 49, 403–409 (2013). [PubMed: 23590310]
8. Calvier L, Legchenko E, Grimm L, Sallmon H, Hatch A, Plouffe BD, Schroeder C, Bauersachs J, Murthy SK, Hansmann G, Galectin-3 and aldosterone as potential tandem biomarkers in pulmonary arterial hypertension. Heart 102, 390–396 (2016). [PubMed: 26869635]
9. Maron BA, Opotowsky AR, Landzberg MJ, Loscalzo J, Waxman AB, Leopold JA, Plasma aldosterone levels are elevated in patients with pulmonary arterial hypertension in the absence of left ventricular heart failure: a pilot study. Eur J Heart Fail 15, 277–283 (2013). [PubMed: 23111998]

10. Maron BA, Zhang YY, White K, Chan SY, Handy DE, Mahoney CE, Loscalzo J, Leopold JA, Aldosterone inactivates the endothelin-B receptor via a cysteinyl thiol redox switch to decrease pulmonary endothelial nitric oxide levels and modulate pulmonary arterial hypertension. Circulation 126, 963–974 (2012). [PubMed: 22787113]
11. Mitts TF, Bunda S, Wang Y, Hinek A, Aldosterone and mineralocorticoid receptor antagonists modulate elastin and collagen deposition in human skin. J Invest Dermatol 130, 2396–2406 (2010). [PubMed: 20535129]
12. Menche J, Sharma A, Kitsak M, Ghiassian SD, Vidal M, Loscalzo J, Barabási AL, Disease networks. Uncovering disease-disease relationships through the incomplete interactome. Science 347, 1257601 (2015). [PubMed: 25700523]
13. Sekizawa N, Yoshimoto T, Hayakawa E, Suzuki N, Sugiyama T, Hirata Y, Transcriptome analysis of aldosterone-regulated genes in human vascular endothelial cell lines stably expressing mineralocorticoid receptor. Mol Cell Endocrinol 341, 78–88 (2011). [PubMed: 21664252]
14. Katayose T, Iwata S, Oyaizu N, Hosono O, Yamada T, Dang NH, Hatano R, Tanaka H, Ohnuma K, Morimoto C, The role of Cas-L/NEDD9 as a regulator of collagen-induced arthritis in a murine model. Biochem Biophys Res Commun 460, 1069–1075 (2015). [PubMed: 25847598]
15. Omata Y, Nakamura S, Koyama T, Yasui T, Hirose J, Izawa N, Matsumoto T, Imai Y, Seo S, Kurokawa M, Tsutsumi S, Kadono Y, Morimoto C, Aburatani H, Miyamoto T, Tanaka S, Identification of Nedd9 as a TGF-beta-Smad2/3 Target Gene Involved in RANKL-Induced Osteoclastogenesis by Comprehensive Analysis. PLoS One 11, e0157992 (2016). [PubMed: 27336669]
16. Evans JV, Ammer AG, Jett JE, Bolcato CA, Breaux JC, Martin KH, Culp MV, Gannett PM, Weed SA, Src binds cortactin through an SH2 domain cystine-mediated linkage. J Cell Sci 125, 6185–6197 (2012). [PubMed: 23097045]
17. Steiner MK, Syrkina OL, Kolliputi N, Mark EJ, Hales CA, Waxman AB, Interleukin-6 overexpression induces pulmonary hypertension. Circ Res 104, 236–244, 228 p following 244 (2009). [PubMed: 19074475]
18. Kumar R, Mickael C, Kassa B, Gebreab L, Robinson JC, Koyanagi DE, Sanders L, Barthel L, Meadows C, Fox D, Irwin D, Li M, McKeon BA, Riddle S, Dale Brown R, Morgan LE, Evans CM, Hernandez-Saavedra D, Bandeira A, Maloney JP, Bull TM, Janssen WJ, Stenmark KR, Tuder RM, Graham BB, TGF-beta activation by bone marrow-derived thrombospondin-1 causes Schistosoma- and hypoxia-induced pulmonary hypertension. Nat Commun 8, 15494 (2017). [PubMed: 28555642]
19. Aghamohammadzadeh R, Zhang YY, Stephens TE, Arons E, Zaman P, Polach KJ, Matar M, Yung LM, Yu PB, Bowman FP, Opotowsky AR, Waxman AB, Loscalzo J, Leopold JA, Maron BA, Up-regulation of the mammalian target of rapamycin complex 1 subunit Raptor by aldosterone induces abnormal pulmonary artery smooth muscle cell survival patterns to promote pulmonary arterial hypertension. FASEB J 30, 2511–2527 (2016). [PubMed: 27006450]
20. Moon JC, Sachdev B, Elkington AG, McKenna WJ, Mehta A, Pennell DJ, Leed PJ, Elliott PM, Gadolinium enhanced cardiovascular magnetic resonance in Anderson-Fabry disease. Evidence for a disease specific abnormality of the myocardial interstitium. Eur Heart J 24, 2151–2155 (2003). [PubMed: 14643276]
21. Ji H, Ramsey MR, Hayes DN, Fan C, McNamara K, Kozlowski P, Torrice C, Wu MC, Shimamura T, Perera SA, Liang MC, Cai D, Naumov GN, Bao L, Contreras CM, Li D, Chen L, Krishnamurthy J, Koivunen J, Chirieac LR, Padera RF, Bronson RT, Lindeman NI, Christiani DC, Lin X, Shapiro GI, Janne PA, Johnson BE, Meyerson M, Kwiatkowski DJ, Castrillon DH, Bardeesy N, Sharpless NE, Wong KK, LKB1 modulates lung cancer differentiation and metastasis. Nature 448, 807–810 (2007). [PubMed: 17676035]
22. Zhou RT, He M, Yu Z, Liang Y, Nie Y, Tai S, Teng CB, Baicalein inhibits pancreatic cancer cell proliferation and invasion via suppression of NEDD9 expression and its downstream Akt and ERK signaling pathways. Oncotarget 8, 56351–56363 (2017). [PubMed: 28915595]
23. Miyake-Nishijima R, Iwata S, Saijo S, Kobayashi H, Kobayashi S, Souta-Kuribara A, Hosono O, Kawasaki H, Tanaka H, Ikeda E, Okada Y, Iwakura Y, Morimoto C, Role of Crk-associated substrate lymphocyte type in the pathophysiology of rheumatoid arthritis in tax transgenic mice and in humans. Arthritis Rheum 48, 1890–1900 (2003). [PubMed: 12847683]

24. Bradbury P, Bach CT, Paul A, O'Neill GM, Src kinase determines the dynamic exchange of the docking protein NEDD9 (neural precursor cell expressed developmentally down-regulated gene 9) at focal adhesions. J Biol Chem 289, 24792–24800 (2014). [PubMed: 25059660]
25. Zheng M, McKeown-Longo PJ, Regulation of HEF1 expression and phosphorylation by TGF-beta 1 and cell adhesion. J Biol Chem 277, 39599–39608 (2002). [PubMed: 12189134]
26. Law SF, Zhang YZ, Klein-Szanto AJ, Golemis EA, Cell cycle-regulated processing of HEF1 to multiple protein forms differentially targeted to multiple subcellular compartments. Mol Cell Biol 18, 3540–51 (1998). [PubMed: 9584194]
27. Leopold JA, Dam A, Maron BA, Scribner AW, Liao R, Handy DE, Stanton RC, Pitt B, Loscalzo J, Aldosterone impairs vascular reactivity by decreasing glucose-6-phosphate dehydrogenase activity. Nat Med 13, 189–197 (2007). [PubMed: 17273168]
28. Das M, Dempsey EC, Reeves JT, Stenmark KR, Selective expansion of fibroblast subpopulations from pulmonary artery adventitia in response to hypoxia. Am J Physiol Lung Cell Mol Physiol 282, L976–986 (2002). [PubMed: 11943662]
29. Hopper RK, Moonen JR, Diebold I, Cao A, Rhodes CJ, Tojais NF, Hennigs JK, Gu M, Wang L, Rabinovitch M, In Pulmonary Arterial Hypertension, Reduced BMPR2 Promotes Endothelial-to-Mesenchymal Transition via HMGA1 and Its Target Slug. Circulation 133, 1783–1794 (2016). [PubMed: 27045138]
30. El Kasmi KC, Pugliese SC, Riddle SR, Roth JM, Anderson AL, Frid MG, Li M, Pullamsetti SS, Savai R, Nagel MA, Fini MA, Graham BB, Tuder RM, Friedman JE, Eltzschig HK, Sokol RJ, Stenmark KR, Adventitial fibroblasts induce a distinct proinflammatory/profibrotic macrophage phenotype in pulmonary hypertension. J Immunol 193, 597–609 (2014). [PubMed: 24928992]
31. Liu F, Haeger CM, Dieffenbach PB, Sicard D, Chrobak I, Coronata AM, Suarez Velandia MM, Vitali S, Colas RA, Norris PC, Marinkovic A, Liu X, Ma J, Rose CD, Lee SJ, Comhair SA, Erzurum SC, McDonald JD, Serhan CN, Walsh SR, Tschumperlin DJ, Fredenburgh LE, Distal vessel stiffening is an early and pivotal mechanobiological regulator of vascular remodeling and pulmonary hypertension. JCI Insight 1, pii: e86987 (2016).
32. Aliotta JM, Pereira M, Wen S, Dooner MS, Del Tatto M, Papa E, Goldberg LR, Baird GL, Ventetuolo CE, Quesenberry PJ, Klinger JR, Exosomes induce and reverse monocrotaline-induced pulmonary hypertension in mice. Cardiovasc Res 110:319–330 (2016). [PubMed: 26980205]
33. Chen F, Li X, Aquadro E, Haigh S, Zhou J, Stepp DW, Weintraub NL, Barman SA, Fulton DJ, Inhibition of histone deacetylase reduces transcription of NADPH oxidases and ROS production and ameliorates pulmonary arterial hypertension. Free Radic Biol Med 99, 167–178 (2016). [PubMed: 27498117]
34. Zhou A, Carrell RW, Murphy MP, Wei Z, Yan Y, Stanley PL, Stein PE, Broughton Pipkin F, Read RJ, A redox switch in angiotensinogen modulates angiotensin release. Nature 468, 108–111 (2010). [PubMed: 20927107]
35. Fessel JP, Flynn CR, Robinson LJ, Penner NL, Gladson S, Kang CJ, Wasserman DH, Hemnes AR, West JD, Hyperoxia synergizes with mutant bone morphogenetic protein receptor 2 to cause metabolic, oxidant injury, and pulmonary hypertension. Am J Respir Cell Mol Biol 49, 778–87 (2013). [PubMed: 23742019]
36. Upton PD, Davies RJ, Tamara T, Morrell NW, Transforming growth factor-β_1 represses bone morphogenetic protein-mediated Smad signaling in pulmonary artery smooth muscle cells via Smad3. Am J Respir Cell Mol Biol 49, 1135–1145 (2013). [PubMed: 23937428]
37. Tuder RM, Archer SL, Dorfmuller P, Erzurum SC, Guignabert C, Michelakis E, Rabinovitch M, Schermuly R, Stenmark KR, Morrell NW, Relevant issues in the pathology and pathobiology of pulmonary hypertension. J Am Coll Cardiol 62, D4–12 (2013). [PubMed: 24355640]
38. Handy DE, Loscalzo J, Responses to reductive stress in the cardiovascular system. Free Radic Biol Med 109, 114–24 (2017). [PubMed: 27940350]
39. Maron BA, Michel T, Subcellular localization of oxidants and redox modulation of endothelial nitric oxide synthase. Circ J 76, 2497–512 (2012). [PubMed: 23075817]
40. Law SF, Estojak J, Wang B, Mysliwiec T, Kruh G, Golemis EA, Human enhancer of filamentation 1, a novel p130cas-like docking protein, associates with focal adhesion kinase and induces

pseudohyphal growth in Saccharomyces cerevisiae. Mol Cell Biol 16, 3327–37 (1996). [PubMed: 8668148]

41. Preston IR, Sagliani KD, Warburton RR, Hill NS, Fanburg BL, Jaffe IZ, Mineralocorticoid receptor antagonism attenuates experimental pulmonary hypertension. Am J Physiol Lung Cell Mol Physiol 304, L678–688 (2013). [PubMed: 23457185]
42. Freeman LC, A set of measures of centrality based on betweenness. Sociometry 40, 35–41 (1977).
43. Biasini M, Bienert S, Waterhouse A, Arnold K, Studer G, Schmidt T, Kiefer F, Gallo Cassarino T, Bertoni M, Bordoli L, Schwede T, SWISS-MODEL: modelling protein tertiary and quaternary structure using evolutionary information. Nucleic Acids Res 42, W252–258 (2014). [PubMed: 24782522]
44. Soylu I, Marino SM, Cy-preds: An algorithm and a web service for the analysis and prediction of cysteine reactivity. Proteins 84, 278–291 (2016). [PubMed: 26685111]
45. Bradbury P, Mahmassani M, Zhong J, Turner K, Paul A, Verrills NM, O'Neill GM, PP2A phosphatase suppresses function of the mesenchymal invasion regulator NEDD9. Biochim Biophys Acta 1823, 290–297 (2012). [PubMed: 22061964]
46. Yung LM, Nikolic I, Paskin-Flerlage SD, Pearsall RS, Kumar R, Yu PB, A Selective Transforming Growth Factor-beta Ligand Trap Attenuates Pulmonary Hypertension. Am J Respir Crit Care Med 194, 1140–1151 (2016). [PubMed: 27115515]
47. Murphy DA, Courtneidge SA, The 'ins' and 'outs' of podosomes and invadopodia: characteristics, formation and function. Nat Rev Mol Cell Biol 12, 413–426 (2011). [PubMed: 21697900]
48. Tsou PS, Balogh B, Pinney AJ, Zakhem G, Lozier A, Amin MA, Stinson WA, Schiopu E, Khanna D, Fox DA, Koch AE, Lipoic acid plays a role in scleroderma: insights obtained from scleroderma dermal fibroblasts. Arthritis Res Ther 16, 411 (2014). [PubMed: 25123250]
49. Shevchenko A, Tomas H, Havlis J, Olsen JV, Mann M, In-gel digestion for mass spectrometric characterization of proteins and proteomes. Nat Protoc 1, 2856–2860 (2006). [PubMed: 17406544]
50. Maron BA, Zhang YY, Handy DE, Beuve A, Tang SS, Loscalzo J, Leopold JA, Aldosterone increases oxidant stress to impair guanylyl cyclase activity by cysteinyl thiol oxidation in vascular smooth muscle cells. J Biol Chem 284, 7665–7672 (2009). [PubMed: 19141618]
51. Peng J, Gygi SP, Proteomics: the move to mixtures. J Mass Spectrom 36, 1083–1091 (2001). [PubMed: 11747101]
52. Saidu NE, Noé G, Cerles O, Cabel L, Kavian-Tessler N, Chouzenoux S, Bahuaud M, Chéreau C, Nicco C, Leroy K, Borghese B, Goldwasser F, Batteux F, Alexandre J, Dimethyl fumarate controls the NRF2/DJ-1 axis in cancer cells: Therapeutic applications. Mol Cancer Ther 16, 529–539 (2017). [PubMed: 28069874]
53. Tran MT, Zsengeller ZK, Berg AH, Khankin EV, Bhasin MK, Kim W, Clish CB, Stillman IE, Karumanchi SA, Rhee EP, Parikh SM, PGC1alpha drives NAD biosynthesis linking oxidative metabolism to renal protection. Nature 531, 528–532 (2016). [PubMed: 26982719]
54. Raof NA, Rajamani D, Chu HC, Gurav A, Johnson JM, LoGerfo FW, Pradhan-Nabzdyk L, Bhasin M, The effects of transfection reagent polyethyleneimine (PEI) and non-targeting control siRNAs on global gene expression in human aortic smooth muscle cells. BMC Genomics 17, 20 (2016). [PubMed: 26728506]
55. Strausberg RL, Feingold EA, Grouse LH, Derge JG, Klausner RD, Collins FS, Wagner L, Shenmen CM, Schuler GD, Altschul SF, Zeeberg B, Buetow KH, Schaefer CF, Bhat NK, Hopkins RF, Jordan H, Moore T, Max SI, Wang J, Hsieh F, Diatchenko L, Marusina K, Farmer AA, Rubin GM, Hong L, Stapleton M, Soares MB, Bonaldo MF, Casavant TL, Scheetz TE, Brownstein MJ, Usdin TB, Toshiyuki S, Carninci P, Prange C, Raha SS, Loquellano NA, Peters GJ, Abramson RD, Mullahy SJ, Bosak SA, McEwan PJ, McKernan KJ, Malek JA, Gunaratne PH, Richards S, Worley KC, Hale S, Garcia AM, Gay LJ, Hulyk SW, Villalon DK, Muzny DM, Sodergren EJ, Lu X, Gibbs RA, Fahey J, Helton E, Ketteman M, Madan A, Rodrigues S, Sanchez A, Whiting M, Madan A, Young AC, Shevchenko Y, Bouffard GG, Blakesley RW, Touchman JW, Green ED, Dickson MC, Rodriguez AC, Grimwood J, Schmutz J, Myers RM, Butterfield YS, Krzywinski MI, Skalska U, Smailus DE, Schnerch A, Schein JE, Jones SJ, Marra MA, Mammalian T Gene Collection Program, Generation and initial analysis of more than 15,000 full-length human and mouse cDNA sequences. Proc Natl Acad Sci U S A 99, 16899–16903 (2002). [PubMed: 12477932]

56. Ponticos M, Partridge T, Black CM, Abraham DJ, Bou-Gharios G, Regulation of collagen type I in vascular smooth muscle cells by competition between Nkx2.5 and deltaEF1/ZEB1. Mol Cell Biol 24, 6151–6161 (2004). [PubMed: 15226419]
57. Chu YS, Dufour S, Thiery JP, Perez E, Pincet F, Johnson-Kendall-Roberts theory applied to living cells. Phys Rev Lett 94, 028102 (2005). [PubMed: 15698233]
58. de Jong OG, Verhaar MC, Chen Y, Vader P, Gremmels H, Posthuma G, Schiffelers RM, Gucek M, van Balkom BW, Cellular stress conditions are reflected in the protein and RNA content of endothelial cell-derived exosomes. J Extracell Vesicles 1, (2012).
59. Graham BB, Chabon J, Gebreab L, Poole J, Debella E, Davis L, Tanaka T, Sanders L, Dropcho N, Bandeira A, Vandivier RW, Champion HC, Butrous G, Wang XJ, Wynn TA, Tuder RM, Transforming growth factor-beta signaling promotes pulmonary hypertension caused by Schistosoma mansoni. Circulation 128, 1354–1364 (2013). [PubMed: 23958565]
60. Seo S, Asai T, Saito T, Suzuki T, Morishita Y, Nakamoto T, Ichikawa M, Yamamoto G, Kawazu M, Yamagata T, Sakai R, Mitani K, Ogawa S, Kurokawa M, Chiba S, Hirai H, Crk-associated substrate lymphocyte type is required for lymphocyte trafficking and marginal zone B cell maintenance. J Immunol 175, 3492–3501 (2005). [PubMed: 16148091]
61. McLendon JM, Joshi SR, Sparks J, Matar M, Fewell JG, Abe K, Oka M, McMurtry IF, Gerthoffer WT, Lipid nanoparticle delivery of a microRNA-145 inhibitor improves experimental pulmonary hypertension. J Control Release 210, 67–75 (2015). [PubMed: 25979327]
62. Song Y, Coleman L, Shi J, Beppu H, Sato K, Walsh K, Loscalzo J, Zhang YY, Inflammation, endothelial injury, and persistent pulmonary hypertension in heterozygous BMPR2-mutant mice. Am J Physiol Heart Circ Physiol 295, H677–690 (2008). [PubMed: 18552156]
63. de Man FS, Handoko ML, van Ballegoij JJ, Schalij I, Bogaards SJ, Postmus PE, van der Velden J, Westerhof N, Paulus WJ, Vonk-Noordegraaf A, Bisoprolol delays progression towards right heart failure in experimental pulmonary hypertension. Circ Heart Fail 5, 97–105 (2012). [PubMed: 22157723]
64. Sagawa K, Maughan L, Suga H, Sunagawa K, Effects of growth and aging of organisms on ESPVR: normalization of E_{es} for heart size In: Cardiac Contraction and the Pressure-Volume Relationship. New York, NY: Oxford; 1988:352–353.
65. Söderberg O, Gullberg M, Jarvius M, Ridderstråle K, Leuchowius KJ, Jarvius J, Wester K, Hydbring P, Bahram F, Larsson LG, Landegren U, Direct observation of individual endogenous protein complexes PLA by proximity ligation. Nat Methods 3, 995–1000 (2006). [PubMed: 17072308]

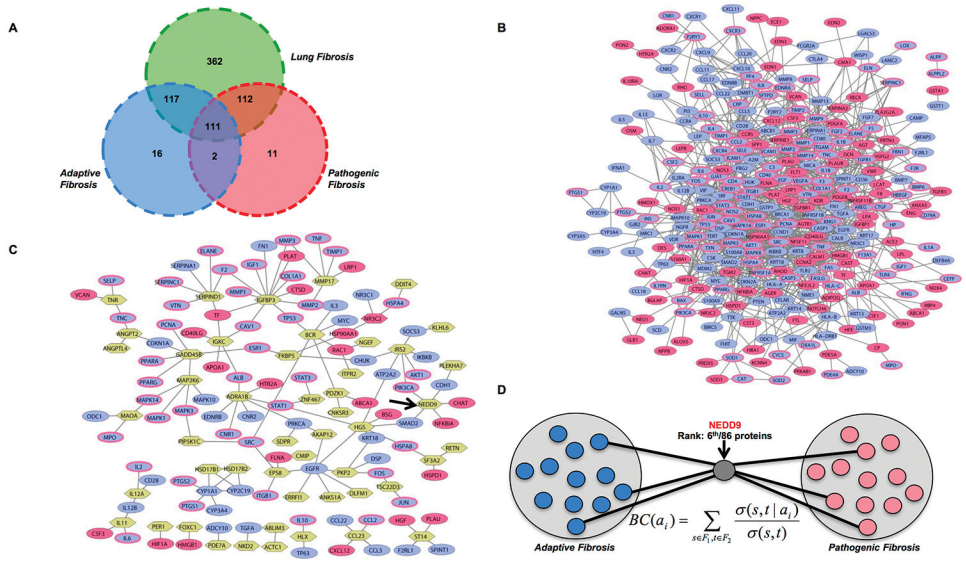

Fig. 1. Betweenness centrality analysis identifies NEDD9 as a critical node regulating the transition between adaptive and pathogenic fibrosis.

(A) Protein-protein interaction network analysis was used to clarify the molecular pathways that regulate two functionally distinct fibrosis subtypes: adaptive and pathogenic. Genes related to dermal and vascular fibrosis were collected from the curated literature, focusing on pulmonary arterial hypertension (PAH) as a human disease correlate to these findings in silico. Genes specifically associated with lung fibrosis ($n = 362$) were excluded from the analysis to limit the probability of analyzing pathways responsible for lung parenchymal fibrosis rather than pulmonary vascular fibrosis. **(B)** The gene products (proteins) associated with adaptive fibrosis (blue), pathogenic fibrosis (red), or both adaptive and pathogenic fibrosis (blue with red border) were mapped to the consolidated human protein-protein interactome (12), resulting in the fibrosome. **(C)** An aldosterone (ALDO)-fibrosome protein-protein interactome subnetwork resulting from associations involving fibrosis genes connected to ALDO-regulated genes. Arrow points to the SMAD3 target and Cas protein NEDD9. **(D)** Betweenness centrality (BC), a measure of importance in information transfer across the network of a node (protein) based on the shortest paths, was used to identify NEDD9 as a critical node in the phenotype transition from adaptive to pathogenic fibrosis. BC of an ALDO-regulated gene (a_i) in connecting adaptive and pathogenic fibrosis (F_1 and F_2, respectively) is the sum of the fraction of all fibrosis gene pairs' shortest paths in the interactome that pass through this ALDO-regulated gene (t) in the interactome, and $\sigma(s,t|a_i)$ is the number of those shortest paths in the interactome that pass through ALDO-regulated gene a_i. The BC score for NEDD9 was ranked 6th of 86 proteins.

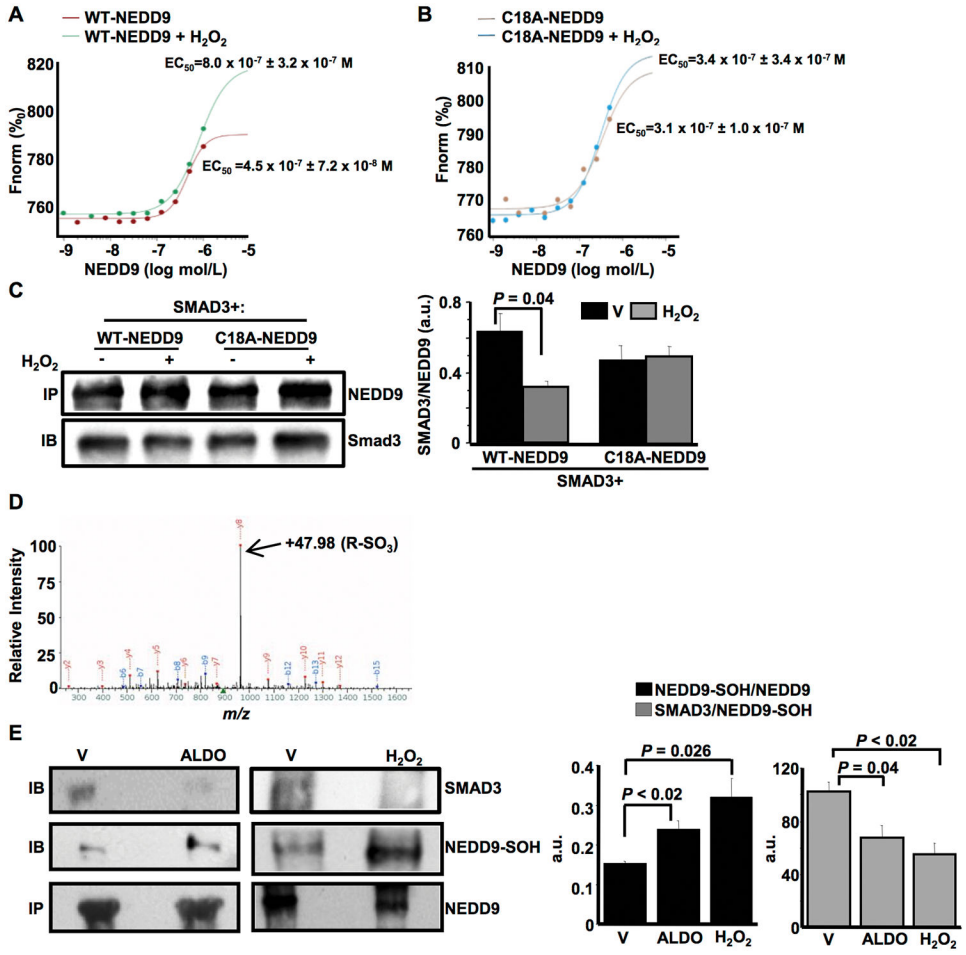

Fig. 2. Oxidation of NEDD9-Cys18 impairs NEDD9-SMAD3 binding.

(A) Hill curves and EC_{50} values of purified wild type (WT) human NEDD9 (0.06 nM–2 μM) or **(B)** mutant NEDD9 containing a substitution of cysteine for alanine at position 18 (C18A-NEDD9, 0.03 nM–1 μM), which is resistant to oxidant stress, incubated with fluorescently labeled SMAD3 (20 nM) in the presence of H_2O_2 (500 μM, 20 min). Data are expressed as EC_{50} ± EC_{50} confidence interval. $n = 2$. **(C)** Immunoprecipitation of COS-7 cells transfected with human DNA coding SMAD3 and WT-NEDD9 or C18A-NEDD9 after treatment with vehicle (V) control, which in this experiment was phosphate-buffered saline, or H_2O_2 (500 μM) for 5 min. NEDD9-SMAD3 binding was calculated by comparing the densitometry ratio of SMAD3 to NEDD9 assessed by immunoblot. Data are from representative immunoblots and expressed as the ratio of SMAD3/NEDD9 in densitometry arbitrary units (a.u.). Means ± SE, $n = 3$–4, Student's unpaired two-tailed *t*-test. **(D)** In-gel trypsin digestion on NEDD9 immunoprecipitated from human pulmonary artery endothelial cells (HPAECs) treated with H_2O_2 (250 μM) for 20 min. Arrow, doubly charged y8 ion corresponding to NEDD9-Cys18 with the addition of three oxygens (-SO_3H) at retention time of 77.3 min and *m/z* value of 944.425 ($n = 3$). **(E)** Immunoprecipitation of NEDD9 from HPAECs treated with vehicle (V) control (DMSO 10^{-7} mol/L), H_2O_2 (250 μM) for 20 min, or aldosterone (ALDO) (10^{-7} mol/L) for 24 hr. Immunoblotting used an antibody against dimedone, detected upon reaction with cysteine sulfenic acid (R-SOH). Data from

representative immunoblots expressed as the ratio of oxidized NEDD9 (NEDD9-SOH)/NEDD9 and the ratio of SMAD3/NEDD9-SOH in a.u.. Means ± SE, $n = 3$, Student's unpaired two-tailed *t*-test. (**C**-**E**) Representative immunoblots and spectra are shown. MS, in-tandem liquid chromatography-mass spectrometry; *m/z*, mass/charge; IB, immunoblot; IP, immunoprecipitation.

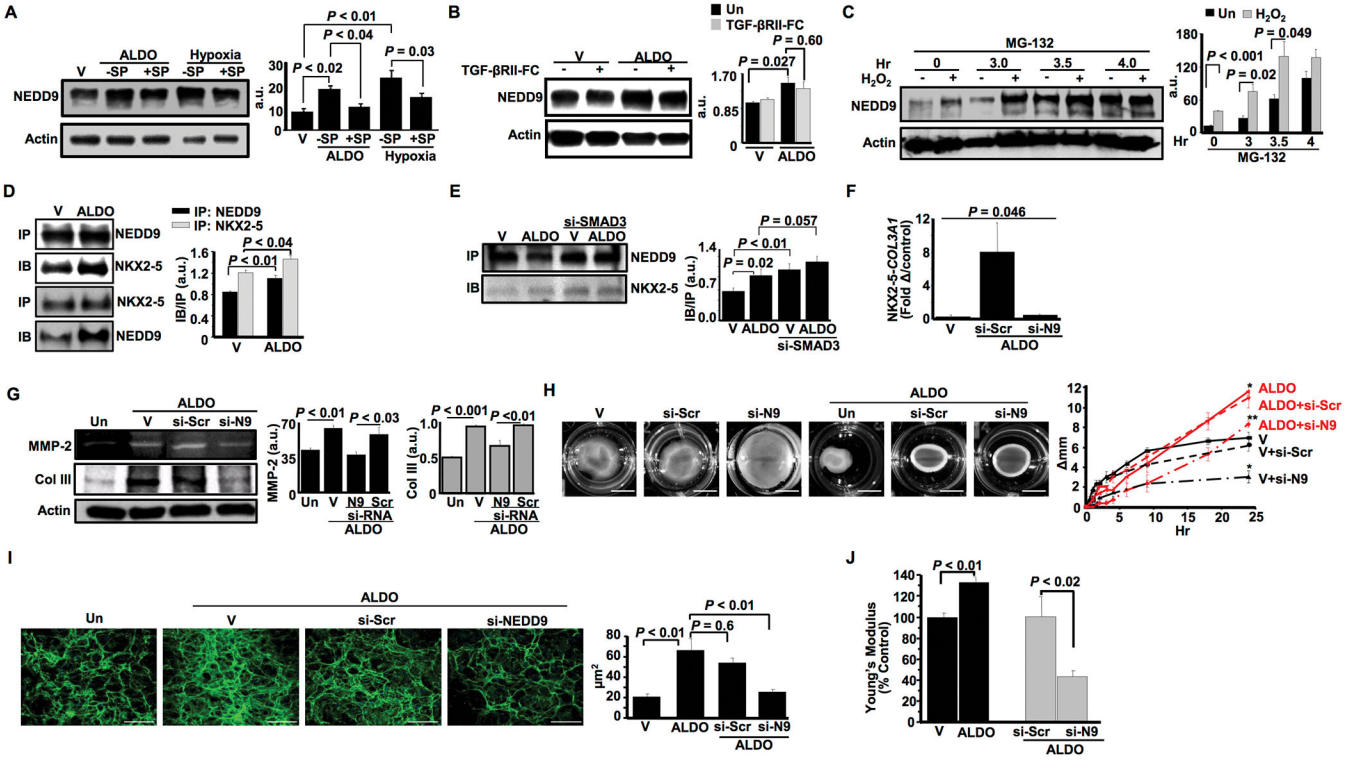

Fig. 3. NEDD9 modulates pulmonary endothelial cell collagen synthesis and fibrosis.

(A) Immunoblot and quantitation in densitometry arbitrary units (a.u.) of NEDD9 form human pulmonary artery endothelial cells (HPAECs) treated with vehicle (V) control, aldosterone (ALDO) (10^{-7} mol/L) for 24 hr, spironolactone (SP) (10 μM) for 24 hr to inhibit ALDO-induced oxidant stress, or hypoxia (FiO_2 0.2%) for 24 hr. Means ± SE, $n = 3$, one-way ANOVA and Tukey's multiple comparisons. The orientation of the hypoxia samples was adjusted for consistency with ALDO samples; however, all bands are from the same blot. **(B)** NEDD9 expression in HPAECs treated with the pan-TGF-β ligand neutralizing antibody TGF-βRII-FC (2.3 μg/mL) for 24 hr prior to treatment with ALDO (10^{-7} mol/L) for 24 hr. Means ± SE, $n = 3$, Student's unpaired two-tailed *t*-test. **(C)** NEDD9 expression in HPAECs pre-treated with the proteasome inhibitor MG-132 (50 μM) for 0–4 hr prior to H_2O_2 (250 μM) for 20 min. Means ± SE, $n = 3$, Student's unpaired two-tailed *t*-test. The orientation of the si-Scr and si-NEDD9 samples was adjusted for consistency; however, all bands are from the same blot. **(D)** Co-immunoprecipitation and quantitation for NEDD9 and the *COL3A1*-targeting transcription factor NKX2–5 from HPAECs incubated with vehicle or ALDO (10^{7} mol/L) for 24 hr. Means ± SE, $n = 3$, Student's unpaired two-tailed *t*-test. In **(E)**, HPAECs were transfected with si-RNA to SMAD3 (si-SMAD3) and the ratio of NKX2–5/NEDD9 is presented in a.u.. Means ± SE, $n = 3$, one-way ANOVA and Tukey's multiple comparisons. **(F)** Chromatin immunoprecipitation of cell lysates using an anti-histone H3 antibody (positive control), immunobeads (negative control), and an anti-NKX2–5 antibody was followed by polymerase chain reaction amplification of the *Col3A1* region containing the NKX2–5 binding site. Data were normalized to positive control and expressed as fold-change for NKX2–5 over negative control. Means ± SE, $n = 3$, one-way ANOVA and Tukey's multiple comparisons. **(G)** MMP-2 proteolytic activity by SDS-PAGE

zymography, collagen III (Col III) expression, and quantitation. (N9, NEDD9); **(H)** images and quantitation of 3-D collagen Matrigel contraction (scale bar = 17.4 mm); **(I)** images and quantitation of collagen fiber content area in um^2 (scale bar = 100 μm); and **(J)** stiffness assessed by atomic force microscopy from HPAECs transfected with si-NEDD9 or si-scrambled (negative) control (si-Scr) and treated with ALDO (10^{-7} mol/L) for 24 hr. (**G-J**) Means ± SE, $n = 3–6$, one-way ANOVA and Tukey's multiple comparisons. *$P < 0.05$ versus V; **$P < 0.05$ versus ALDO. (**A-I**) Representative immunoblots, gels, and micrographs shown. MMP, matrix metalloproteinase; Un, untreated.

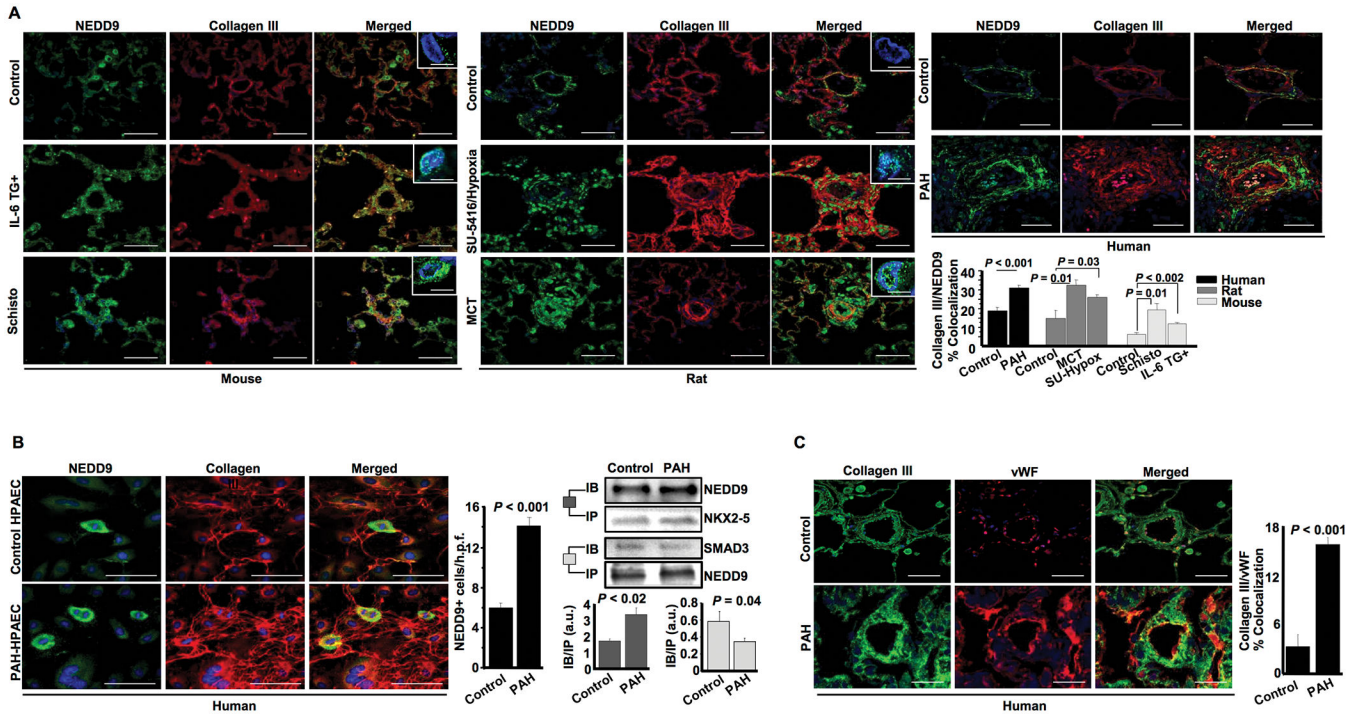

Fig. 4. Pulmonary endothelial NEDD9-collagen III is increased in PAH in vivo.

(A) Immunofluorescence for NEDD9 and collagen III in tissue sections from animal models of PAH [IL-6 TG+ (n = 4), Schisto (n = 4), SU-5416/Hypoxia (n = 5), MCT (n = 5)] and PAH patients (n = 9). Samples from control mice (n = 4) and rats (n = 5), and donor tissue from non-diseased control patients (n = 5) were used for comparison. Insets are merged images for DAPI (blue) and NEDD9 (green) to show nuclear NEDD9 expression; representative images from samples within each condition are provided. Colocalization of collagen III and NEDD9 is expressed as percent double positive area/sum total area of stain for each protein in pulmonary arterioles. Means ± SE, Student's unpaired two-tailed t-test. (**B**) Immunofluorescence for collagen III and NEDD9 in human pulmonary artery endothelial cells (HPAECs) isolated from PAH patients (PAH-HPAEC). Number of NEDD9+ cells per high powered field is quantitated. Co-immunoprecipitation of NEDD9 and NKX2–5 and immunoblot of NEDD9 and SMAD3, with quantitation in densitometry arbitrary units (a.u.). Means ± SE, n = 3–6/group. Student's unpaired two-tailed t-test. **(C)** Collagen III-vWF co-localization in remodeled PAH pulmonary arterioles, expressed as percent double positive area/sum total area of stain for each protein in pulmonary arterioles. Means ± SE, n = 3–5/group, Student's unpaired two-tailed t-test. IP, immunoprecipitation; IB, immunoblot; vWF, Von Willebrand Factor; PAH, pulmonary arterial hypertension; h.p.f., high powered field (200×). Scale bar = 50 μm, Inset scale bar = 4 μm. Representative micrographs and immunoblots shown.

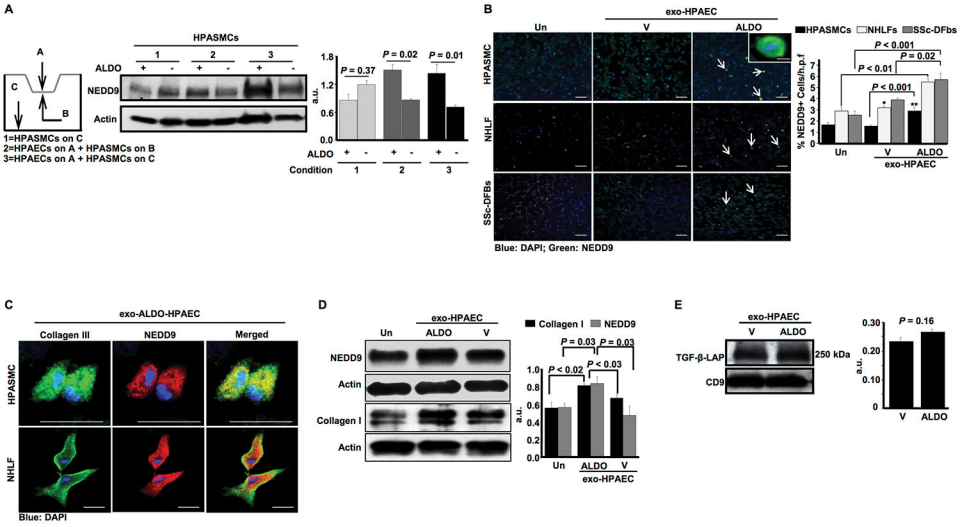

Fig. 5. Exosomes from ALDO-treated HPAECs increase NEDD9 and fibrillar collagen in HPASMCs.

(A) Schematic of culture conditions and representative immunoblots of NEDD9 from human pulmonary artery smooth muscle cells (HPASMCs) co-cultured with human pulmonary artery endothelial cell (HPAECs), treated with aldosterone (ALDO) (10^{-7} mol/L) for 24 hr. Data are expressed as densitometry arbitrary units (a.u.). Means ± SE, $n = 3$, one-way ANOVA and Tukey's multiple comparisons. **(B)** Quantification of NEDD9 positivity in HPASMCs, normal human lung fibroblasts (NHLFs), and dermal fibroblasts from patients with systemic sclerosis without PAH (SSc-DFBs) that were untreated (Un) or treated with exosomes isolated from vehicle (V) (DMSO 10^{-7} mol/L)-treated or aldosterone (ALDO) (10^{-7} mol/L)-treated HPAECs. Data are expressed as % of cells that were NEDD9+ per h.p.f. (200×) (white arrows). exo-HPAEC, exosomes isolated from HPAECs. Inset, representative NEDD9+ cell. Means ± SE, $n = 3$–4, one-way ANOVA and Tukey's multiple comparisons. Scale bar = 100 μm for representative micrographs, scale bar for inset=10 μm. *$P < 0.01$ versus NHLF exo-HPAEC ALDO; **$P < 0.001$ versus HPASMC Un. **(C)** Colocalization of NEDD9 and collagen III in the perinuclear regions of cells undergoing mitotic division in HPASMCs and NHLFs treated with exosomes from ALDO-treated HPAECs (exo-ALDO-HPAEC). $n = 3$. Scale bar = 20 μm. **(D)** Immunoblot of NEDD9 and collagen I in HPASMCs treated with exo-ALDO-HPAEC. Data are expressed in densitometry a.u.. Means ± SE, $n = 4$ for NEDD9; $n = 4$ for collagen I, Student's unpaired two-tailed *t*-test. **(E)** Representative immunoblots of exosomal TGF-β-LAP (TGF-β latent complex) secreted by HPAECs treated with V control and ALDO (10^{-7} mol/L) for 24 hr. Means ± SE, $n = 3$. Student's unpaired two-tailed *t*-test.

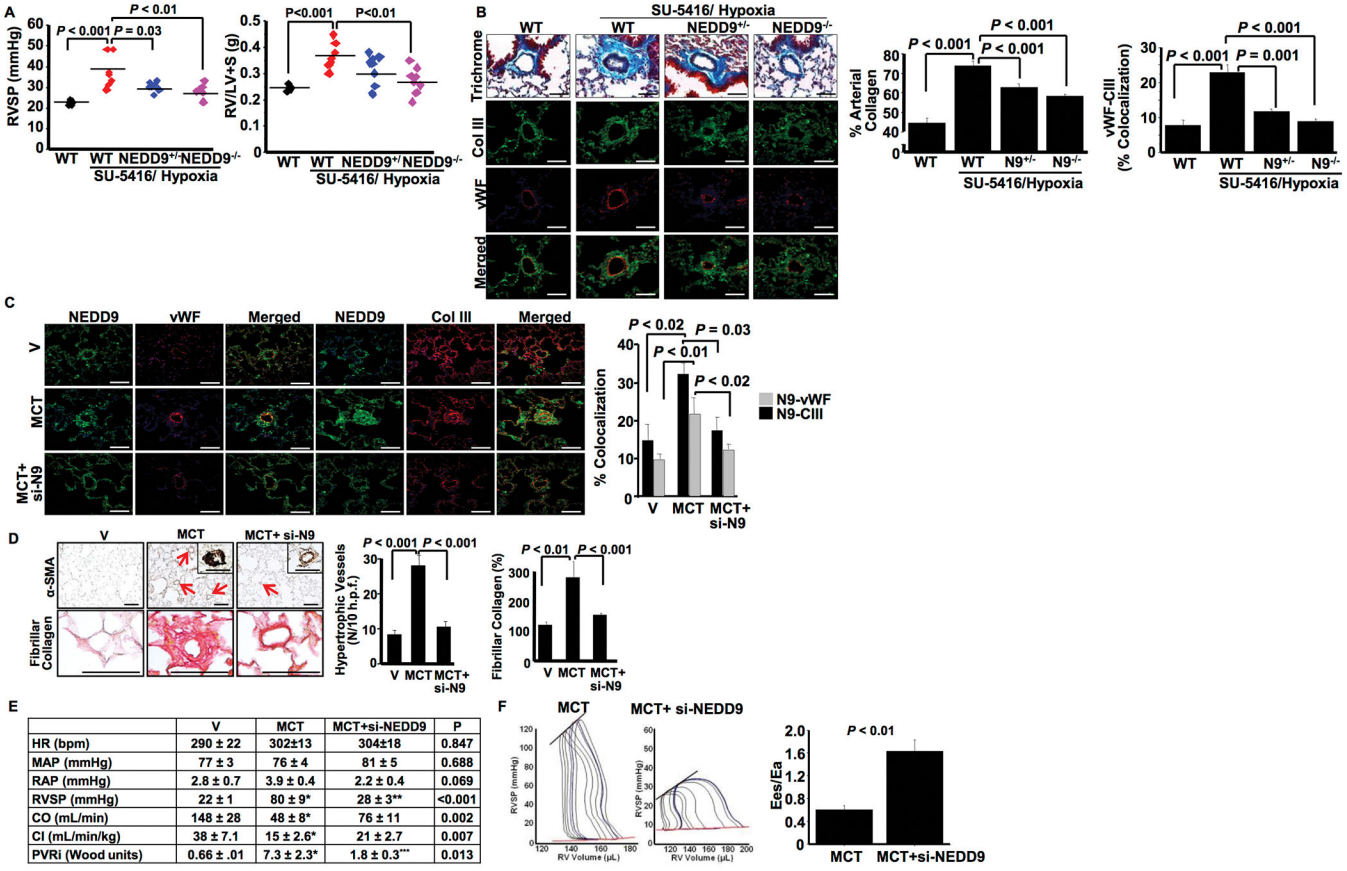

	V	MCT	MCT+si-NEDD9	P
HR (bpm)	290 ± 22	302±13	304±18	0.847
MAP (mmHg)	77 ± 3	76 ± 4	81 ± 5	0.688
RAP (mmHg)	2.8 ± 0.7	3.9 ± 0.4	2.2 ± 0.4	0.069
RVSP (mmHg)	22 ± 1	80 ± 9*	28 ± 3**	<0.001
CO (mL/min)	148 ± 28	48 ± 8*	76 ± 11	0.002
CI (mL/min/kg)	38 ± 7.1	15 ± 2.6*	21 ± 2.7	0.007
PVRi (Wood units)	0.66 ± .01	7.3 ± 2.3*	1.8 ± 0.3**	0.013

Fig. 6. Gene ablation or molecular inhibition of NEDD9 prevented vascular fibrosis and PAH in vivo.

(A) Right ventricular systolic pressure (RVSP) and RV mass by Fulton index (RV/LV + S) in male and female C57BL (WT), C57BL/NEDD9$^{+/-}$, and C57BL/NEDD9$^{-/-}$ mice injected with Sugen-5416 (20 mg/kg) every 7 days during a 3-week period of hypoxia treatment (FiO_2 10%). Means ± SE, n = 6–9 mice/condition for RVSP, n =5–10 mice/condition for heart weight, one-way ANOVA and Tukey's multiple comparisons. **(B)** Representative images of Gomori trichrome staining to assess vascular fibrosis burden and vWF-collagen III colocalization, expressed as percent double positive area/sum total area of stain for each protein, of pulmonary arterioles (20–50 μm in diameter, adjacent to terminal bronchiole) from WT, NEDD9$^{+/-}$, and NEDD9$^{-/-}$ mice treated with or without SU-5416/Hypoxia. Means ± SE, n = 6–10 mice/condition for trichrome; n = 4–7 mice/condition for vWF-collagen III, one-way ANOVA and Tukey's multiple comparisons. Scale bar = 50 μm. Col III, collagen III. **(C)** NEDD9-collagen III and NEDD9-vWF colocalization in lung tissue from male Sprague Dawley rats administrated monocrotaline (MCT) (50 mg/kg) and treated with Staramine-mPEG (1.5 mg/kg) formulated with NEDD9 siRNA (si-NEDD9). Means ± SE, n = 4–5 rats/condition, one-way ANOVA and Tukey's multiple comparisons Scale bar = 50 μm. **(D)** The number of hypertrophic vessels/high powered field (red arrow) and percent vascular fibrillar collagen in paraffin-embedded lung sections was analyzed using anti-α-smooth muscle actin (SMA) immunohistochemistry and Picrosirius Red staining, respectively, from vehicle-, MCT-, and MCT + si-NEDD9-treated rats. Means ± SE, n = 4–5

rats/condition, one-way ANOVA and Tukey's multiple comparisons. Scale bar = 100 μm. Inset, representative hypertrophic vessel magnified, scale bar = 50 μm. **(E)** Table of phenotypic changes in V, MCT, and MCT + si-NEDD9-treated rats. Means ± SE, $n = 5–7$ rats/condition. P values in column represent one-way ANOVA. *$P < 0.05$ versus V, **$P < 0.001$ versus MCT; ***$P = 0.02$ versus MCT by Tukey's multiple comparisons. **(F)** Representative RV pressure-volume loops are show to quantify RV-pulmonary artery coupling, assessed by the ratio of end-systolic elastance (Ees)/pulmonary vascular elastance (Ea) in MCT and MCT + si-NEDD9-treated rats. Means ± SE, $n = 3$ rats/condition, Student's unpaired two-tailed t-test. h.p.f, high power fields (200×). N9, NEDD9; HR, heart rate; MAP, mean arterial pressure; RAP, right atrial pressure; CI, cardiac index; CO, cardiac output, indexed pulmonary vascular resistance (PVRi) in Wood units.